Thin Solid Films 557 (2014) 342–345

Contents lists available at ScienceDirect

Thin Solid Films

journal homepage: www.elsevier.com/locate/tsf

Fabrication and evaluation of propagation loss of Si/SiGe/Si photonic-wire waveguides for Si based optical modulator

Younghyun Kim [a,*], Mitsuru Takenaka [a], Takenori Osada [b], Masahiko Hata [b], Shinichi Takagi [a]

[a] Department of Electrical Engineering and Information Systems, The University of Tokyo, 7-3-1 Hongo, Bunkyo-ku, Tokyo 113-8656, Japan
[b] Sumitomo Chemical Co. Ltd., 6 Kitahara, Tsukuba, Ibaraki 300-3294, Japan

ARTICLE INFO

Available online 25 October 2013

Keywords:
Si/SiGe/Si optical modulator
Si/SiGe/Si heterostructure
Si/SiGe/Si photonic-wire waveguide
Si/SiGe/Si waveguide core
Strained SiGe
Bandgap narrowing
Si-based optical modulator
Optoelectronic integrated circuits

ABSTRACT

We have characterized photonic-wire waveguides with Si/SiGe/Si heterostructure ribs for Si-based optical modulators. The Si (80 nm)/$Si_{0.72}Ge_{0.28}$ (40 nm) layers grown on Si-on-insulator by molecular beam epitaxy for optical modulators were evaluated by *in-situ* reflection high-energy electron diffraction, atomic force microscope, X-ray diffraction and Raman spectroscopy, exhibiting that the fully-strained highly-crystalline SiGe layer was obtained. We have evaluated the propagation loss of the Si/strained SiGe/Si photonic-wire waveguides. The wavelength dependence of the propagation loss exhibits the bandgap narrowing of the strained $Si_{0.72}Ge_{0.28}$, while the optical absorption of the strained $Si_{0.72}Ge_{0.28}$ is not significant for the optical modulator application at 1.55-μm wavelength.

1. Introduction

Recently, silicon (Si) optical modulators have attracted much attention as one of the fundamental building blocks for optoelectronic integrated circuits toward large-scaled integrated circuits with on-chip optical interconnects [1–3]. High speed optical modulators have recently been demonstrated so far by using a Mach–Zehnder interferometer (MZI) with phase-shifters in which the effective refractive index of the Si waveguide is modulated by the electrical signal. An MZI has been mostly used for getting optical modulation because of its wide wavelength bandwidth, while the large device length of several millimeters is considered as one of the most challenging problems for large scale integration [4–6].

To solve this problem, strained SiGe-based optical modulators have been proposed [7,8]. The refractive index change from the plasma dispersion effect is inversely proportional to conductivity effective masses of electrons and holes [9]. Therefore, the lighter conductivity masses become, the larger plasma dispersion occurs. Compressively strained SiGe, which is one of the promising materials for future scaled p-channel metal-oxide-semiconductor (MOS) transistors [10–12], is well known to exhibit the light conductivity hole mass. Thus, the plasma dispersion effect is expected to be enhanced through effective mass modulation in strained SiGe, enabling small device footprint. In our previous work [8], the strain effect on carrier-injection type optical modulators by using the Si/strained SiGe/Si waveguide is numerically investigated. Owing to enhancement in free-carrier effects, the plasma dispersion effect and free-carrier absorption, of strained SiGe, the pin-junction Si/$SiGe_{0.28}$/Si optical modulator has approximately 4.5× smaller switching power than that of the Si modulator. However, the bandgap energy decreases with an increase in the Ge fraction of SiGe, causing an increase in optical absorption at 1.55-μm wavelength [13,14]. In this paper, we have fabricated Si/strained $Si_{0.72}Ge_{0.28}$/Si heterostructures on a silicon-on-insulator (SOI) wafer by molecular beam epitaxy (MBE), and evaluated the propagation loss of the Si/SiGe/Si photonic-wire waveguides for optical modulator applications at 1.55-μm wavelength.

2. Experiment

2.1. Device fabrication

We show the process flow of the Si/SiGe/Si photonic-wire waveguide in Fig. 1. The Si/SiGe/Si–OI substrate was prepared by using a (001) SOI wafer with a 2-μm-thick buried oxide layer (BOX). First, a 220-nm-thick SOI layer was thinned to be 100 nm by thermal oxidation at 1100 °C and BHF etching of a thermally grown SiO_2 layer as shown in Fig. 1(a) and (b). Then, a 40-nm-thick $Si_{0.72}Ge_{0.28}$ layer and an 80-nm-thick Si layer were grown on the SOI by MBE under the base pressure of 3×10^{-8} Pa at 400 °C and 600 °C, respectively as shown in Fig. 1(c). The thickness of the SiGe layer was kept below the critical thickness for avoiding strain relaxation [15]. Then, photonic-wire waveguides with a Si/SiGe mesa were fabricated by using the Si/SiGe/Si–OI wafer. After cleaning the substrate, the electron beam resist (ZEP520A) was coated on the substrate with the spin condition of 3000 rpm for 30 s followed by the prebake at 160 °C for 10 min and deep ultraviolet (DUV) lithography. Then, waveguide patterns of variable waveguide widths were formed by reactive ion etching

* Corresponding author.
E-mail address: yhkim@mosfet.t.u-tokyo.ac.jp (Y. Kim).

0040-6090/$ – see front matter © 2013 Elsevier B.V. All rights reserved.
http://dx.doi.org/10.1016/j.tsf.2013.10.063

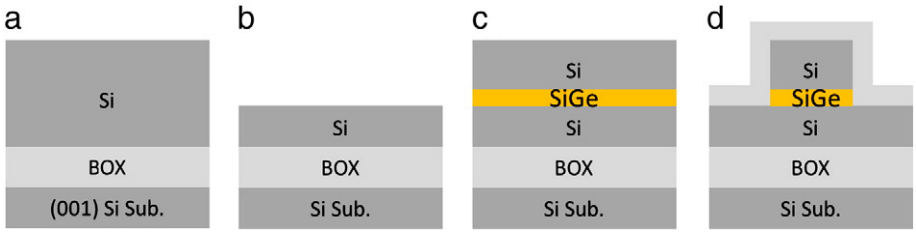

Fig. 1. Process flow of Si/SiGe/Si photonic-wire waveguide. (a) initial 220-nm-thick SOI, (b) 100-nm-thick SOI thinned by thermal oxidation, (c) Si/SiGe/Si–OI grown by MBE, and (d) dry etching of waveguide mesa, followed by SiO_2 passivation.

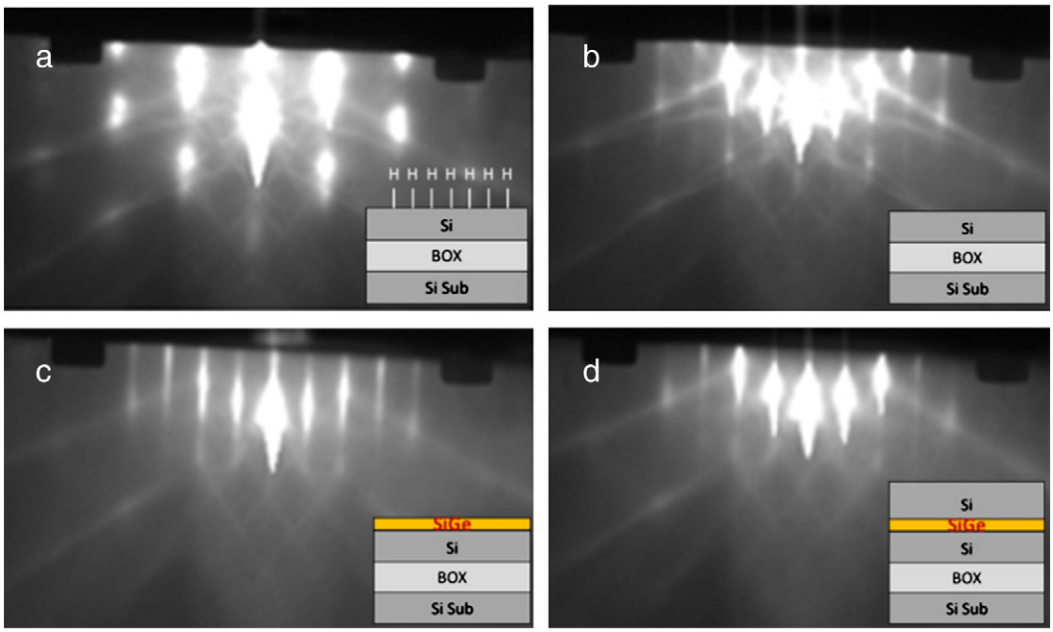

Fig. 2. *in-situ* RHEED images during MBE growth procedures: after (a) SOI installation, (b) thermal cleaning, (c) SiGe growth, and (d) Si growth.

with CF_4 gas for approximately 11 min. The gas pressure of CF_4 and RF power were set to be 1 Pa and 20 W, respectively. Finally, a 500-nm-thick SiO_2 layer was deposited by plasma-enhanced chemical vapor deposition for device passivation as shown in Fig. 1(d). Si photonic-wire waveguides as a control sample were also fabricated by using the 220-nm-thick SOI substrate, which is corresponding to the total thickness of the 80-nm-thick Si/40-nm-thick SiGe/100-nm-thick Si waveguide.

2.2. Characterization of epitaxially grown Si/SiGe/Si–OI and device

Fig. 2 shows the *in-situ* reflection high-energy electron diffraction (RHEED) images during the crystal growth process of Si/SiGe on the SOI substrate. The as-installed sample shows the spotty 1×1 RHEED pattern due to hydrogen termination during BHF as shown in Fig. 2(a). Fig. 2(b) shows the longish 2×1 RHEED pattern after thermal cleaning at 850 °C for 30 min, meaning that hydrogen was removed by high thermal energy. Fig. 2(c) and (d) show the longish 2×1 RHEED patterns during the SiGe and Si growth, indicating the two dimensional island morphology.

Fig. 3 shows the surface morphologies of the Si/SiGe/SOI substrate measured by atomic force microscope (AFM, Nanocute SS, Dynamic force mode). The root-mean-squares of the surface roughness with the scanning areas of (a) $500 \times 500\ nm^2$, (b) $5 \times 5\ \mu m^2$, and (c) $10 \times 10\ \mu m^2$ are less than 0.18 nm, indicating that the pseudomorphic strained SiGe layer is obtained.

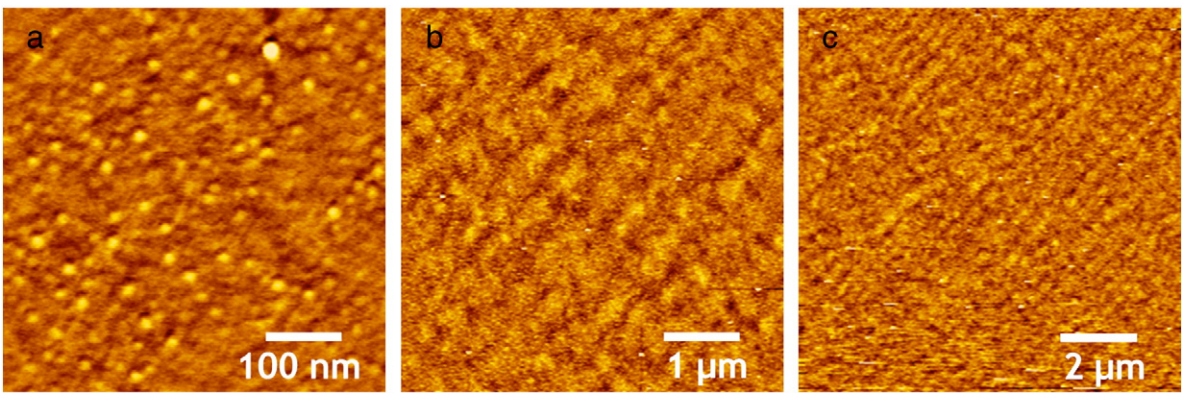

Fig. 3. AFM evaluation of surface roughnesses of the Si/SiGe/SOI samples grown by MBE with the scanning areas of (a) $500 \times 500\ nm^2$, (b) $5 \times 5\ \mu m^2$, and (c) $10 \times 10\ \mu m^2$.

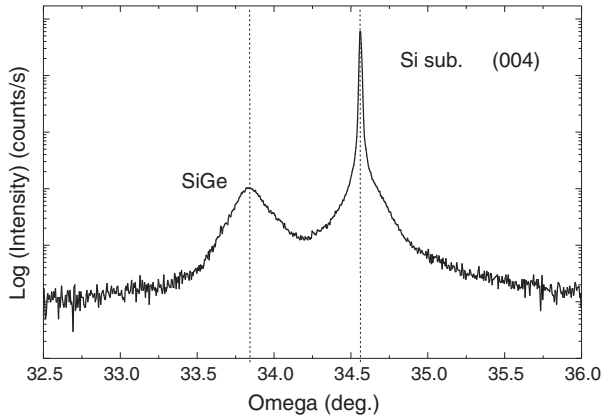

Fig. 4. ω-2θ profiles around the (004) x-ray diffraction of the Si/SiGe/SOI.

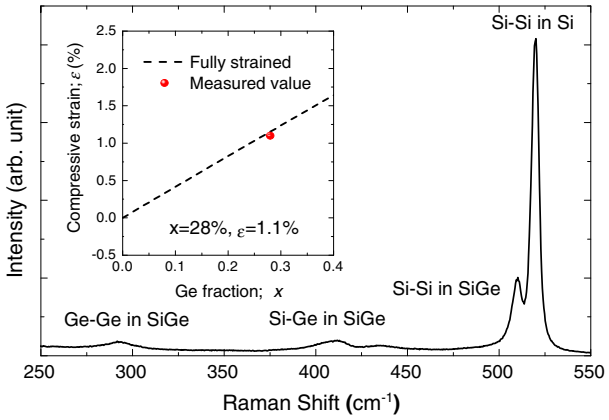

Fig. 5. Raman spectrum of Si/SiGe/Si–OI. The inset is the measured compressive strain as a function of the Ge fraction.

To investigate the crystal quality of the grown SiGe layer, we measured the ω-2θ profile of Si/SiGe/SOI substrate by using x-ray diffraction (XRD, X'Pert PRO MRD, 1.8 kW, Kα1). The x-ray diffraction peak of the SiGe layer was clearly observed with the peak of the Si substrate (004) shown in Fig. 4. From the angle of diffraction, the lattice constant of SiGe normal to the surface was estimated to be 5.532 Å, much larger than that of a relaxed $Si_{0.72}Ge_{0.28}$, 5.489 Å. Thus, the compressive strain is estimated to be as large as 1.0% when the Ge fraction of the SiGe alloy is 28%.

The Si/SiGe/Si–OI substrate was also evaluated by Raman spectroscopy (LabRAM HR, 488 nm) to precisely evaluate the Ge fraction and strain value in the SiGe layer by using the method depicted in Ref. [16]. The Raman spectrum of the SiGe layer shown in Fig. 5 exhibits the three major phonon modes corresponding to the Si–Si, Si–Ge, and Ge–Ge bonds. It is found from Fig. 5 that the Ge fraction and the compressive strain value of the SiGe layer is approximately 28% and 1.1% respectively, which means that the SiGe layer is almost fully strained as indicated in the inset of Fig. 5.

Fig. 6(a) and (b) show the cross-sectional and bird's-eye view scanning electron microscope (SEM, S-4700, 10 kV) images of the Si/SiGe/Si photonic-wire waveguide, clearly indicating a well-defined core without excessive lateral over-etching in the SiGe layer.

To investigate the absorption related to the bandgap of the strained SiGe, the wavelength dependence of the Si/SiGe/Si photonic-wire waveguide loss was measured from 1340 nm (0.761 eV) to 1630 nm (0.925 eV). A continuous-wave (CW) light from tunable laser sources coupled the waveguide through a lensed fiber with a spot size of approximately 4 μm. The input light is adjusted to TE-polarized light by using an in-line polarizer. The output light from the waveguide was collected by an objective lens and coupled again to a single-mode optical fiber. The output power was monitored by an InGaAs photodetector. Here, it has been reported that SiGe waveguides has nonlinear optical properties, which is dependent on the power of laser [17]. However, in our experiment, the power of laser coupled to waveguides is small enough for suppressing such a nonlinear effect described in [17]. The power of laser coupled to waveguides is approximately −10 dBm (0.1 mW) by taking a coupling loss into account, which is smaller than that discussed in Ref. [17] by three orders of magnitude.

The device length was approximately 1 cm. Fig. 7 shows that the absorption of the Si/SiGe/Si waveguide increases with an increase in the photon energy due to the indirect bandgap of $Si_{0.72}Ge_{0.28}$ near 0.88 eV [18]. The propagation loss at 1.55-μm wavelength, which is the most important wavelength for optical communications, was also measured by the cut-back method with variable waveguide width as shown in Fig. 8. The propagation loss dramatically increases in both SiGe and Si waveguides as the width decreases due to the sidewall roughness arising from DUV lithography. The width dependence loss is known by the theoretical model in which the loss was expressed to be inversely proportional to the width squared [19]. The propagation loss based on the theoretical model can be expressed by

$$\text{propagation loss} = \frac{\sigma}{w^2} + \text{offset} \quad (1)$$

where, σ is the fitting parameter related to surface roughness, w is the width of a waveguide, and "offset" is additional loss from

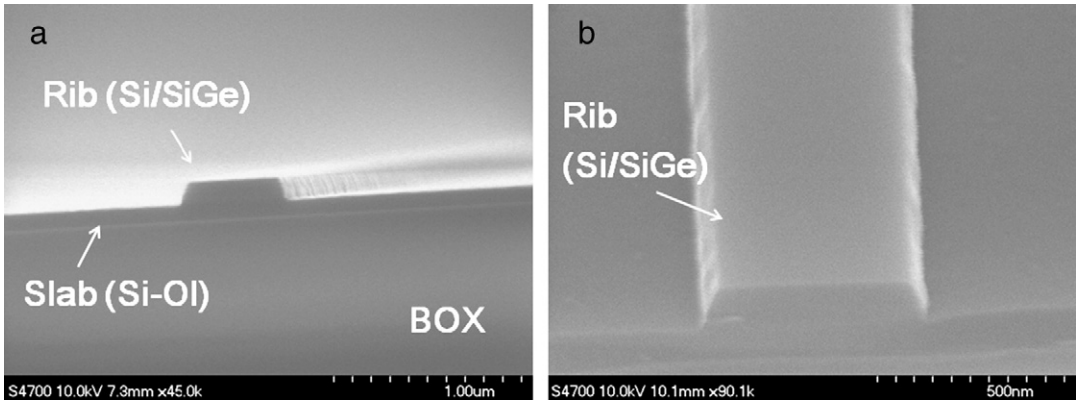

Fig. 6. SEM images of the fabricated optical waveguide with Si/SiGe mesa: (a) tilted-cross-sectional view and (b) tilted-bird's-eye view.

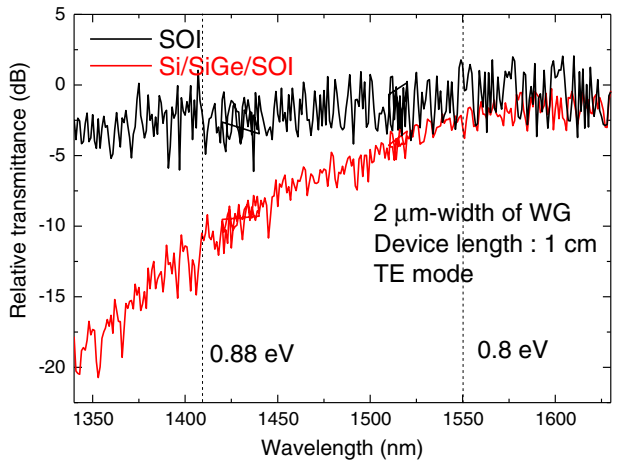

Fig. 7. Wavelength dependence of propagation loss in 2 μm-width Si and Si/SiGe/Si photonic-wire waveguides. The device length is approximately 1 cm.

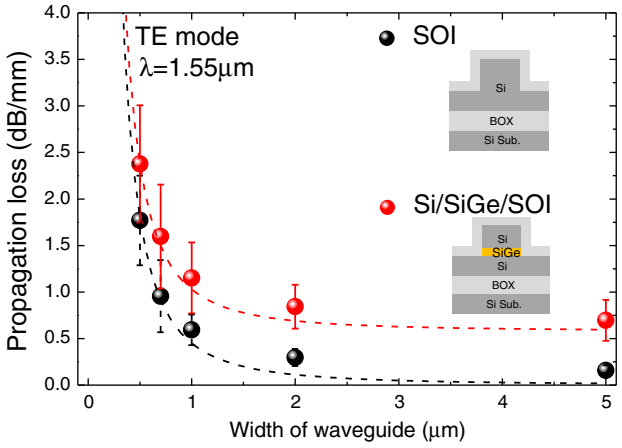

Fig. 8. Propagation losses of Si and Si/SiGe/Si waveguides as a function of the waveguide width measured by the cut-back method and schematic of the waveguides (inset).

band-to-band absorption. The experimental results of the width dependence losses of the Si/$SiGe_{0.28}$/Si and Si waveguides were fitted by using the fitting parameters in Eq. (1) to the model in which the loss was expressed to be inversely proportional to the square of width.

The numerical fitting was carried out for the Si and Si/SiGe/Si waveguide with the model. We found that the increases in the propagation loss with a decrease in waveguide width less than 1 μm are almost same for the Si and Si/SiGe/Si waveguides. In addition, we observed the difference in the propagation loss between the Si and Si/SiGe/Si waveguides with 5-μm width even though the sidewall-roughness-induced loss is almost negligible in case of the large-width waveguide. Therefore, we can conclude that the sidewall-roughness-induced losses for the Si and Si/SiGe/Si waveguide are almost same and the estimation of the band-to-band absorption in the SiGe layer is not affected by the sidewall roughness of the waveguides.

The ratio of σ of between the Si/$SiGe_{0.28}$/Si and Si waveguides is nearly one, meaning that the surface-roughness-induced losses are almost same. On the other hand, offset of Si/$SiGe_{0.28}$/Si is 0.54 while offset of Si is almost 0; we assumed the constant offset loss in the model because the band-to-band absorption in the SiGe layer was not dependent on the waveguide width. Hence, the additional loss caused by the absorption in the compressively strained $Si_{0.72}Ge_{0.28}$ layer is estimated to be 0.54 dB/mm (1.2 cm^{-1}) at 1.55 μm. Although the propagation loss of the Si/SiGe/Si waveguide is higher than the typical Si waveguides loss of less than 0.3 dB/mm, we can monolithically integrate a Si/SiGe/Si layer for active regions and a Si layer for passive regions by using selective area growth. Thus, we can avoid additional propagation loss in the passive area. In addition, the increase in the propagation loss of the Si/SiGe/Si modulators is not significant because the length of the modulator can be reduced by the enhanced plasma dispersion effect in strained SiGe.

3. Conclusion

We have fabricated the Si/SiGe/Si waveguide on an SOI substrate by using MBE. The wavelength and waveguide's width dependences of the propagation loss of the Si/SiGe/Si photonic-wire waveguides reveal that the additional propagation loss related to the narrow bandgap in the fully strained $Si_{0.72}Ge_{0.28}$ layer is approximately 0.54 dB/mm at 1.55-μm wavelength, which is negligible for optical modulator applications.

Acknowledgment

This work was partly supported by the Strategic Information and Communications R&D Promotion Programme of the Ministry of Internal Affairs and Communications.

References

[1] A. Liu, M. Paniccia, Phys. E. 35 (2006) 223.
[2] C. Gunn, IEEE Micro. 26 (2006) 58.
[3] G.T. Reed, G. Mashanovich, F.Y. Gardes, D.J. Thomson, Nat. Photonics 4 (2010) 518.
[4] L. Liao, A. Liu, D. Rubin, J. Basak, Y. Chetrit, H. Nguyen, R. Cohen, N. Izhaky, M. Paniccia, Electron. Lett. 43 (2007) 1196.
[5] F.Y. Gardes, D.J. Thomson, N.G. Emerson, G.T. Reed, Opt. Express 19 (2011) 11804.
[6] D.J. Thomson, F.Y. Gardes, J.-M. Fedeli, S. Zlatanovic, Y. Hu, B.P.P. Kuo, E. Myslivets, N. Alic, S. Radic, G.Z. Mashanovich, G.T. Reed, IEEE Photon. Technol. Lett. 24 (2012) 234.
[7] M. Takenaka, S. Takagi, IEEE J. Sel. Top. Quantum Electron. 48 (2012) 8.
[8] Y. Kim, M. Takenaka, S. Takagi, San Diego, U.S.A., September 29, 2012, 9th Conf. of Group IV Photonics, Proceedings WP18, 2012, p. 126.
[9] R.A. Soref, B.R. Bennett, IEEE J. Quantum Electron. 23 (1987) 123.
[10] M.V. Fischetti, S.E. Laux, J. Appl. Phys. 80 (1996) 2234.
[11] T. Manku, J.M. McGregor, A. Nathan, D.J. Roulston, J.P. Noel, D.C. Houghton, IEEE Trans. Electron Devices 40 (1993) 1990.
[12] K. Cheng, A. Khakifirooz, N. Loubet, S. Luning, T. Nagumo, M. Vinet, Q. Liu, A. Reznicek, T. Adam, S. Naczas, P. Hashemi, J. Kuss, J. Li, H. He, L. Edge, J. Gimbert, P. Khare, Y. Zhu, Z. Zhu, A. Madan, N. Klymko, S. Holmes, T.M. Levin, A. Hubbard, R. Johnson, M. Terrizzi, S. Teehan, A. Upham, G. Pfeiffer, T. Wu, A. Inada, F. Allibert, B.-Y. Nguyen, L. Grenouillet, Y. Le Tiec, R. Wacquez, W. Kleemeier, R. Sampson, R.H. Dennard, T.H. Ning, M. Khare, G. Shahidi, B. Doris, Electron Devices Meeting (IEDM), 2012 IEEE International (2012)18.1.1-18.1.4.
[13] R. Braunstein, A.R. Moore, F. Herman, Phys. Rev. 109 (1958) 695.
[14] D.V. Lang, R. People, J.C. Bean, A.M. Sergent, Appl. Phys. Lett. 47 (1985) 1333.
[15] R. People, J.C. Bean, Appl. Phys. Lett. 47 (1985) 322.
[16] F. Pezzoli, E. Bonera, E. Grilli, M. Guzzii, S. Sanguinetti, D. Chrastina, G. Isella, H.v. Känel, E. Wintersberger, J. Stangl, G. Bauer, Mater. Sci. Semicond. Process. 11 (2008) 279.
[17] K. Hammani, M.A. Ettabib, A. Borgris, A. Kapsalis, D. Syvridis, M. Brun, P. Labeye, S. Nicoletti, D.J. Richardson, P. Petropulos, Opt. Express 21 (2013) 16690.
[18] J.C. Bean, Proc. IEEE 80 (1992) 571.
[19] F.P. Payme, J.P.R. Lacey, Opt. Quant. Electron. 26 (1994) 977.